Submitted to ADVANCED MATERIALS

Submitted to ADVANCED MATERIALS

DOI: 10.1002/adma.((please add manuscript number))
Article type: Communication

Stimulus-Responsive Micro-Supercapacitors with Ultrahigh Energy Density and Reversible Electrochromic Window

By *Panpan Zhang, Feng Zhu, Faxing Wang, Jinhui Wang, Renhao Dong, Xiaodong Zhuang*, Oliver G. Schmidt, and Xinliang Feng**

P. Zhang, F. Wang, Dr. R. Dong, Dr. X. Zhuang, Prof. X. Feng
Center for Advancing Electronics Dresden (cfaed) & Department of Chemistry and Food Chemistry, Technische Universität Dresden, 01062 Dresden, Germany.
E-mail: xinliang.feng@tu-dresden.de
Dr. F. Zhu, J. Wang, Prof. O. G. Schmidt
Material Systems for Nanoelectronics, Chemnitz University of Technology, Reichenhainer Str. 70, 09107 Chemnitz, Germany.
Prof. O. G. Schmidt
Center for Advancing Electronics Dresden (cfaed), Technische Universität Dresden, 01062 Dresden, Germany.
Dr. X. Zhuang, Prof. X. Feng
School of Chemistry and Chemical Engineering, Shanghai Jiao Tong University, 200240 Shanghai, P. R. China.
E-mail: zhuang@sjtu.edu.cn

Keywords: micro-supercapacitor, stimulus-responsive, in-plane, flexible, viologen

Smart micro-/nano-devices or stimuli-responsive devices, which can be engineered to respond to a variety of inputs, such as pH, ions, heat, light, magnetic field, etc., have attracted substantial attention due to a wide range of needs for smart modern electronics.[1] Such kind of stimuli-responsive devices play an increasingly vital role in modern optoelectronic, biomimic, and energy-related devices.[2] Thus far, polyurethane, Prussian blue, and albumin-coated MnO_2 have been used for self-healing supercapacitor, electrochromic battery, and pH/H_2O_2 dual-responsive nanocarrier for tumor, respectively.[2a, 2e, 2f] Nevertheless, it remains a great challenge to integrate various kinds of stimuli into modern functional devices without sacrificing the device performance, most probably due to the poor compatibility among those stimuli, active materials and processing technologies.

Increasing interest in portable and implantable electronic devices has triggered great demand for micro-sized energy storage devices (MESDs)[3], due to the heavy energy consumption, device miniaturization and silicon technology compatibility requirements.[4] Among those MESDs, micro-supercapacitors (MSCs) are one kind of new-generation micro-sized power sources and have attracted considerable attention due to their small size, controllable patterning and excellent electrochemical performance.[5] Importantly, on-chip MSCs can be directly integrated in-plane with other thin film energy-generating or storage devices, such as piezoelectric devices, triboelectric devices, and batteries, to produce sustainable power systems.[6] Therefore, the development of on-chip MSCs with high areal/volumetric capacitances, high energy/power densities, high rate capability as well as flexibility[7] are the main scientific pursue in recent years.

In this work, we demonstrate the fabrication of the first stimulus-responsive MSC (SR-MSC) with a reversible electrochromic window. Taking advantage of the synergistic effect of one-dimensional (1D) V_2O_5 nanoribbons and two-dimensional (2D) exfoliated graphene (EG) nanosheets, EG/V_2O_5 hybrid nanopaper was prepared as electrode for MSCs, which delivered a high volumetric capacitance of 130.7 F cm^{-3} at 10 mV s^{-1} with a polyvinyl alcohol (PVA)/LiCl gel electrolyte. Notably, the volumetric energy density was approximately 20 mWh cm^{-3} (power density = 235 mW cm^{-3}), which is markedly higher than the energy densities of the state-of-the-art MSCs. After solidification of the electrolyte together with methyl viologen, the resulting SR-MSCs manifested a remarkable reversible electrochromic effect during the charge–discharge process within 0-1 V, which provided a direct visual observation of the charge–discharge state of the MSCs.

The EG nanosheets and V_2O_5 nanoribbons were firstly prepared using an electrochemical exfoliation method and a hydrothermal method, respectively.[8] The EG/V_2O_5 hybrid film was obtained through facile vacuum filtration of a dispersion of EG and V_2O_5 mixture (mass ratio

= 4:1, Figure S1). Subsequently, the hybrid film was transferred onto transparent substrates such as rigid glass slide or flexible polyethylene terephthalate (PET) film. The transmittances of transparent substrate-supported EG/V_2O_5 hybrid nanopapers reached 45% (Figure S2). The fabrication process for MSCs is schematically illustrated in **Figure 1**. First, the substrate-supported EG/V_2O_5 hybrid film was patterned by gold interdigital electrodes through a mask (Figure 1a and 1b, details about the Au electrodes deposition were illustrated in Figure 1f and S3). The uncovered area was then removed through sequential O_2 plasma and HCl solution etching (Figure 1c). Second, methyl viologen (MV^{2+}, Figure 1e) dissolved PVA/LiCl gel electrolyte was drop-casted on the surface of the interdigital electrodes and solidified overnight (Figure 1d). Finally, an all-solid-state EG/V_2O_5 hybrid film-based in-plane MSC (EG/V_2O_5-MSC) was constructed (Figure 1h and 1i). For comparison, pure EG or V_2O_5 film based MSCs (EG-MSC or V_2O_5-MSC, respectively) were also fabricated by applying the same procedure.

The morphologies of the EG nanosheets, V_2O_5 nanoribbons, and EG/V_2O_5 hybrid film were inspected by using atomic force microscopy (AFM), scanning electron microscope (SEM) and high-resolution transmission electron microscopy (HRTEM). The AFM image and height profile for EG nanosheets indicate that the EG nanosheets own lateral size of 2–5 μm and average thickness of 2.0 nm (Figure S4), corresponding to 2~3 layers of graphene sheets.[9] HRTEM images shown in Figure S5 reveal the hexagonal crystalline structure of a typical bilayer graphene sheet. In contrast, V_2O_5 exhibits ribbon-like morphology with a width of 50–200 nm and length of 5–10 μm (Figure S6); further inspection of the HRTEM and SAED images manifest that the nanoribbons are single crystalline with well-defined lattices (Figure S7).[10] The top-view SEM image of EG/V_2O_5 hybrid film exhibits the presence of both folded EG nanosheets and V_2O_5 nanoribbons (Figure S8), in contrast to the pristine EG film or V_2O_5 film (Figure S9). The SEM and HRTEM images of the EG/V_2O_5 hybrid nanopaper (Figure 1g,

and S10-12) clearly show a nanosheet–nanoribbon interlaced conformation. In addition, the sheet resistance for EG/V_2O_5 hybrid nanopaper measured by a four-point probe system reveals a mean value of 1.73 kΩ sq^{-1}, which is comparable with that of pristine EG film (1.34 kΩ sq^{-1}). The XRD patterns of EG/V_2O_5 film (Figure S13) show an intense peak at 26.1° and a series of XRD peaks from 6.4 to 38.5°, respectively, which suggest an interlayer *d*-spacing of 3.41 Å for EG and high crystalline layered structure for V_2O_5.[11] The resulting EG/V_2O_5 hybrid film was further characterized by Raman spectroscopy and X-ray photoelectron spectroscopy (Figure S14 and S15).

Cyclic voltammograms (CV) measurement (Figure S16) was first performed to evaluate the electrochemical performance of as-fabricated MSCs on glass substrates. The V_2O_5-MSC exhibited similar two pairs of redox peaks in the range of 0–1.0 V in comparison with that measured in three-electrode cells (Figure S17), which can be ascribed to the intercalation and deintercalation of Li^+ ions from V_2O_5 nanoribbons lattice[12] (Figure S18), and accompanied by the electrochemical conversion of V^{5+} to various valence states. The EG-MSC displayed ideal rectangular CV curves, indicating typical electric double layer capacitive (EDLC) behavior. In contrast, the EG/V_2O_5-MSC exhibited non-strict rectangular shape, due to the combination of an EDLC material (EG) and a pseudo-capacitance material (V_2O_5), especially at low current densities.[12-13] The EG/V_2O_5-MSC possessed a substantially higher current density than those for EG-MSC and V_2O_5-MSC at the same scan rate, suggesting much enhanced capacitance for the former device (**Figure 2**a). According to these CV curves at different scan rates, the areal and volumetric capacitances (C_A and C_V) of EG/V_2O_5-MSC were calculated (Figure 2b). Notably, the C_V for EG/V_2O_5-MSC reached 130.7 F cm^{-3} at the rate of 10 mV s^{-1}, which is much higher than those of reported MSCs, such as, 1.3 F cm^{-3} for carbon onions,[3b] 17.9 F cm^{-3} for graphene,[5b] 1.08 F cm^{-3} for a graphene–carbon nanotube (CNT) carpet,[5a] 3.1 F cm^{-3} for graphene-CNT,[14] 20.4 F cm^{-3} for CNT-carbon-MnO_2,[15] 4.42 F cm^{-3}

for graphene/MnO_2/Ag nanowire (NW),[16] and 105 F cm^{-3} for polyaniline NW.[17] On the other hand, the C_A for EG/V_2O_5-MSC at 10 mV s^{-1} reached 3.92 mF cm^{-2}, which is well comparable with most of previously reported MSCs (Table S1).[5b, 18]

The capacitive behavior of the fabricated MSCs was further studied by using galvanostatic charge–discharge (GCD) measurement at current densities from 0.02 to 8 mA cm^{-2} (Figure S19). Significant internal resistance (IR) drops reflecting the poor conductivity and large resistance of the V_2O_5 electrode can be observed for V_2O_5-MSC. In contrast, almost no IR drop was observed for EG/V_2O_5-MSC (Figure 2c). On the basis of the discharge curve, the specific areal and volumetric capacitances of EG/V_2O_5-MSC (Figure S20) were calculated to be 2.3 mF cm^{-2} and 76.7 F cm^{-3} at a current density of 0.02 mA cm^{-2}, respectively, both of which are superior to those for EG-MSC (C_A: 0.1 mF cm^{-2}; C_V: 3.3 F cm^{-3}) and V_2O_5-MSC (C_A: 0.34 mF cm^{-2}; C_V: 11.3 F cm^{-3}). The enhanced performance for EG/V_2O_5-MSC can be attributed to synergistic effect of two components: V_2O_5 nanoribbons acted as "spacers" to prevent the aggregation of EG nanosheets in the hybrid film and promoted the accessibility of electrolytes for the hybrid film (Figure S21), while the EG layers improved the electrical conductivity of the whole hybrid electrode.

In order to understand the excellent electrochemical performances of EG/V_2O_5-MSC, its electrochemical impedance spectra (EIS) were further studied (Figure S22). EG/V_2O_5-MSC exhibited almost overlapped and near-vertical line intersection with the real axis at low frequency (inset of Figure S22) in comparison with EG-MSC, suggesting fast ion diffusion within EG/V_2O_5-MSC which benefited from the presence of EG component. At high frequency, EG/V_2O_5-MSC exhibited lower charge transfer resistance (13.2 Ω) than that for V_2O_5-MSC (18.3 Ω), suggesting rapid ion transport for EG/V_2O_5-MSC.[19] The dependence of the phase angles on the frequencies of as-prepared MSCs are presented in Figure 2d. The characteristic frequency f_0 at the phase angle of -45° for the EG/V_2O_5-MSC was 18,516 Hz,

which is much higher than the values for the V_2O_5-MSC (1,518 Hz) and EG-MSC (13,906 Hz). Therefore, the corresponding time constant τ_0 ($\tau_0 = 1/f_0$), which refers to the minimum time necessary to discharge all the energy from the device with an efficiency of more than 45%, was calculated as only 0.05 ms for EG/V_2O_5-MSC in comparison with those for EG-MSC (0.07 ms) and V_2O_5-MSC (0.66 ms).[3b, 20] These results strongly suggested that the EG/V_2O_5-MSC possessed eminent potential for the instantaneous delivery of ultrahigh power and energy.

To demonstrate the overall performance of the EG/V_2O_5-MSC, Ragone plots were calculated (Figure 2e and S23). Notably, EG/V_2O_5-MSC delivered volumetric energy density of up to 20 mWh cm^{-3} at 0.75 W cm^{-3}, which is one order of magnitude higher than that of typical activated carbon based supercapacitor (< 1 mWh cm^{-3})[20] and lithium thin-film batteries (10^{-3}–10^{-2} Wh cm^{-3})[3b]. In addition, EG/V_2O_5-MSC also provided ultrahigh power density of up to 235 W cm^{-3} at 0.07 mWh cm^{-3}, which is approximately 25 times higher than that of conventional supercapacitors and even comparable with that of high-power electrolytic capacitors (10^1–10^3 W cm^{-3}).[20] These results for EG/V_2O_5-MSC are superior to most of graphene-based MSCs (Table S1), eg. graphene-based MSCs,[18b] graphene-CNT carpet-based MSCs,[5a] polyaniline NW MSCs,[17] graphene-CNT MSCs,[14] and graphene/MnO_2/Ag NW MSCs[16]. Moreover, EG/V_2O_5-MSC also showed a long-term stability with 93% capacitance retention up to 6000 charge-discharge cycles at 0.04 mA cm^{-2} (Figure 2f).

To realize the stimulus-responsive function for the as-prepared flexible MSCs, viologen, which is one kind of electrochromic molecules, was chosen as the key stimulus molecule by directly adding it into electrolyte (Figure 1e). The fabrication process for SR-MSC on flexible substrate (PET) is fully compatible to that for non-responsive MSCs. The PET-supported hybrid nanopaper exhibited good uniformity, flexibility and favorable transparency (45% transmittance, Figure S2). Remarkably, the fabricated EG/V_2O_5 based flexible MSC

(EG/V_2O_5-fMSC) exhibited *in-situ* reversible electrochromic phenomenon during the charge-discharge cycles between 0 and 1.0 V (**Figure 3**a), which can be explained by the electrically driven equilibrium (Figure 1e and S24) between the viologen (MV^{2+}, colorless) and the radical ion derivative of viologen (MV^{+}, purple, Figure 1e) in the LiCl electrolyte.[21] This electrochromic function for MSCs can be expanded by using other electrochromic additives, such as polyaniline, polythiphene, polypyrrole and rare earth metal coordinated compounds.[22] In addition, compared with glass-supported MSCs, the PET-supported SR-MSCs retained a similar CV shape at scan rates from 10 to 2000 mV s^{-1} (Figure S25), indicating the unaffected electrochemical performance with different substrates. The CV curves for the PET-supported SR-MSC were then examined at a scan rate of 10 mV s^{-1} at four bending angles (0^o, 30^o, 60^o, and 90^o in Figure 3b). No obvious changes were observed for the CV curves under different bending states (Figure 3c), highlighting the good flexibility and electrochemical stability for the PET-supported devices.

The electrochromic effect of the EG/V_2O_5-fMSC was further investigated using an *in-situ* UV-vis spectro-electrochemical technique to monitor the absorbance changes at 550 nm in response to an applied GCD voltage (at 0.01 mA cm^{-2}, Figure 3d and S26). During the 3-min charging process, the color of the EG/V_2O_5-fMSC gradually became deeper and the absorbance increased, indicating the transformation from MV^{2+} to MV^{+}. When the voltage reached 1 V, the deepest purple color could be observed and the highest absorbance represented the conversion from MV^{2+} to MV^{+}. During the charging/discharging, as-fabricated electrochromic MSCs can be considered as stimulus-responsive MSCs due to the absorbance changing under external applied voltage. During the 3-min discharging, EG/V_2O_5-fMSC began to fade until colorless at 0 V (Figure 3d). Thereby, the charge-discharge cycle and corresponding absorbance changes at different voltages offered the direct visual observation of energy storage states. Such colorless-purple shuttling during charge-discharge

process could be realized at low current density of 0.01 mA cm^{-2} (**Figure 4**a). In addition, after 200 charge-discharge cycles at high current density of 0.4 mA cm^{-2}, the absorbance of the EG/V_2O_5-fMSC remained no obvious change according to the *in-situ* monitored UV-Vis spectra (at 550 nm, Figure 4b). All these results suggested good cycle stability of the SR-MSCs at both low and high current densities. Most importantly, the response time of the SR-MSCs could be controlled from several minutes to only a few seconds at the current densities from 0.01 to 0.4 mA cm^{-2} (Figure 4c). Thus, ultrafast response performance could be achieved under high charge-discharge current densities.

In summary, we demonstrate the first stimulus-responsive MSCs with ultrahigh energy density and ultra-fast responsive time by using viologen and EG/V_2O_5 hybrid nanopaper as stimulus-responsive material and electrode, respectively. The high volumetric capacitance of 130.7 F cm^{-3} at 10 mV s^{-1} and high volumetric energy density (20 mWh cm^{-3} at 235 mW cm^{-3}), as well as long lifetime cycling performance of the fabricated SR-MSCs can be attributed to the synergistic role offered by V_2O_5 nanoribbons and EG nanosheets. The fabricated SR-MSCs exhibited 0-1.0 V reversible electrochromic effect during charge–discharge cycles, not only offering direct visualization of the energy storage state without the aid of extra techniques, but also making it possible for enhanced human-device interaction experience in the future.

Supporting Information
Supporting Information is available online from the Wiley Online Library or from the author.

Acknowledgements
The authors thank the financial support from the German Research Foundation (DFG) within the Cluster of Excellence ‘Center for Advancing Electronics Dresden’ (cfaed) and financed by the Initiative and Networking Fund of the German Helmholtz Association, Helmholtz International Research School for Nanoelectronic Networks NanoNet (VH-KO-606), ERC Grant on 2DMATER, UP-GREEN and EU Graphene Flagship. We acknowledge the use of the facilities in the Dresden Center for Nanoanalysis at the Technische Universität Dresden.

Received: ((will be filled in by the editorial staff))
Revised: ((will be filled in by the editorial staff))
Published online: ((will be filled in by the editorial staff))

[1] a) M. A. C. Stuart, W. T. S. Huck, J. Genzer, M. Müller, C. Ober, M. Stamm, G. B. Sukhorukov, I. Szleifer, V. V. Tsukruk, M. Urban, F. Winnik, S. Zauscher, I. Luzinov, S. Minko, *Nat. Mater.* **2010**, *9*, 101; b) D. Roy, J. N. Cambre, B. S. Sumerlin, *Prog. Polym. Sci.* **2010**, *35*, 278; c) M. K. Tsang, G. Bai, J. Hao, *Chem. Soc. Rev.* **2015**, *44*, 1585; d) J. Thévenot, H. Oliveira, O. Sandre, S. Lecommandoux, *Chem. Soc. Rev.* **2013**, *42*, 7099; e) E. G. Kelley, J. N. Albert, M. O. Sullivan, I. T. H. Epps, *Chem. Soc. Rev.* **2013**, *42*, 7057.

[2] a) Y. Huang, Y. Huang, M. Zhu, W. Meng, Z. Pei, C. Liu, H. Hu, C. Zhi, *ACS Nano* **2015**, *9*, 6242; b) H. Wang, B. Zhu, W. Jiang, Y. Yang, W. R. Leow, H. Wang, X. Chen, *Adv. Mater.* **2014**, *26*, 3638; c) C. O'Dwyer, *Adv. Mater.* **2016**, *28*, 5681; d) D. Qi, Z. Liu, Y. Liu, W. R. Leow, B. Zhu, H. Yang, J. Yu, W. Wang, H. Wang, S. Yin, X. Chen, *Adv. Mater.* **2015**, *27*, 5559; e) J. Wang, L. Zhang, L. Yu, Z. Jiao, H. Xie, X. W. Lou, X. Wei Sun, *Nat. Commun.* **2014**, *5*, 5921; f) Q. Chen, L. Feng, J. Liu, W. Zhu, Z. Dong, Y. Wu, Z. Liu, *Adv. Mater.* **2016**, *28*, 7129; g) Q. Jiang, N. Kurra, H. N. Alshareef, *Adv. Funct. Mater.* **2015**, *25*, 4976.

[3] a) P. Simon, Y. Gogotsi, *Nat. Mater.* **2008**, *7*, 845; b) D. Pech, M. Brunet, H. Durou, P. Huang, V. Mochalin, Y. Gogotsi, P.-L. Taberna, P. Simon, *Nat. Nanotechnol.* **2010**, *5*, 651; c) G. Xiong, C. Meng, R. G. Reifenberger, P. P. Irazoqui, T. S. Fisher, *Electroanalysis* **2014**, *26*, 30; d) X. Wang, Y. Chen, O. G. Schmidt, C. Yan, *Chem. Soc. Rev.* **2016**, *45*, 1308; e) W. Si, C. Yan, Y. Chen, S. Oswald, L. Han, O. G. Schmidt, *Energy Environ. Sci.* **2013**, *6*, 3218; f) B. Wang, X. Fang, H. Sun, S. He, J. Ren, Y. Zhang, H. Peng, *Adv. Mater.* **2015**, *27*, 7854.

[4] a) J. Chmiola, C. Largeot, P.-L. Taberna, P. Simon, Y. Gogotsi, *Science* **2010**, *328*, 480; b) P. Huang, C. Lethien, S. Pinaud, K. Brousse, R. Laloo, V. Turq, M. Respaud, A. Demortière, B. Daffos, P. L. Taberna, B. Chaudret, Y. Gogotsi, P. Simon, *Science* **2016**, *351*, 691; c) X. Zhuang, X. Feng, *Angew. Chem. Int. Ed.* **2016**, *55*, 6136; d) S. Liu, P. Gordiichuk, Z. S. Wu, Z. Liu, W. Wei, M. Wagner, N. Mohamed-Noriega, D. Wu, Y. Mai, A. Herrmann, K. Müllen, X. Feng, *Nat. Commun.* **2015**, *6*, 8817.

[5] a) J. Lin, C. Zhang, Z. Yan, Y. Zhu, Z. Peng, R. H. Hauge, D. Natelson, J. M. Tour, *Nano Lett.* **2013**, *13*, 72; b) Z. S. Wu, K. Parvez, X. Feng, K. Müllen, *Nat. Commun.* **2013**, *4*, 2487.

[6] D. Kim, D. Kim, H. Lee, Y. R. Jeong, S.-J. Lee, G. Yang, H. Kim, G. Lee, S. Jeon, G. Zi, J. Kim, J. S. Ha, *Adv. Mater.* **2016**, *28*, 748.

[7] a) Y. Shao, M. F. El-Kady, L. J. Wang, Q. Zhang, Y. Li, H. Wang, M. F. Mousavi, R. B. Kaner, *Chem. Soc. Rev.* **2015**, *44*, 3639; b) Z. Niu, L. Zhang, L. Liu, B. Zhu, H. Dong, X. Chen, *Adv. Mater.* **2013**, *25*, 4035; c) Z. Liu, Z.-S. Wu, S. Yang, R. Dong, X. Feng, K. Müllen, *Adv. Mater.* **2016**, *28*, 2217; d) Z.-S. Wu, K. Parvez, S. Li, S. Yang, Z. Liu, S. Liu, X. Feng, K. Müllen, *Adv. Mater.* **2015**, *27*, 4054.

[8] a) K. Parvez, Z. S. Wu, R. Li, X. Liu, R. Graf, X. Feng, K. Müllen, *J. Am. Chem. Soc.* **2014**, *136*, 6083; b) S. Yang, S. Brüller, Z.-S. Wu, Z. Liu, K. Parvez, R. Dong, F. Richard, P. Samorì, X. Feng, K. Müllen, *J. Am. Chem. Soc.* **2015**, *137*, 13927; c) J. Zhu, L. Cao, Y. Wu, Y. Gong, Z. Liu, H. E. Hoster, Y. Zhang, S. Zhang, S. Yang, Q. Yan, P. M. Ajayan, R. Vajtai, *Nano Lett.* **2013**, *13*, 5408.

[9] C. Lee, X. Wei, J. W. Kysar, J. Hone, *Science* **2008**, *321*, 385.

[10] X. Rui, Z. Lu, H. Yu, D. Yang, H. H. Hng, T. M. Lim, Q. Yan, *Nanoscale* **2013**, *5*, 556.

[11] a) T. Yao, Y. Oka, N. Yamamoto, *Mat. Res. Bull.* **1992**, *27*, 669; b) C.-C. Hu, K.-H. Chang, *Electrochem. Solid-State Lett.* **2004**, *7*, A400; c) L. Cao, J. Zhu, Y. Li, P. Xiao, Y. Zhang, S. Zhang, S. Yang, *J. Mater. Chem. A* **2014**, *2*, 13136.

[12] Q. T. Qu, Y. Shi, L. L. Li, W. L. Guo, Y. P. Wu, H. P. Zhang, S. Y. Guan, R. Holze, *Electrochem. Commun.* **2009**, *11*, 1325.

[13] G. Wang, X. Lu, Y. Ling, T. Zhai, H. Wang, Y. Tong, Y. Li, *ACS Nano* **2012**, *6*, 10296.

[14] M. Beidaghi, C. Wang, *Adv. Funct. Mater.* **2012**, *22*, 4501.

[15] L. Sun, X. Wang, K. Zhang, J. Zou, Q. Zhang, *Nano Energy* **2016**, *22*, 11.

[16] W. Liu, C. Lu, X. Wang, R. Y. Tay, B. K. Tay, *ACS Nano* **2015**, *9*, 1528.

[17] C. Meng, J. Maeng, S. W. M. John, P. P. Irazoqui, *Adv. Energy Mater.* **2014**, *4*, 1301269.

[18] a) J. Lin, Z. Peng, Y. Liu, F. Ruiz-Zepeda, R. Ye, E. L. Samuel, M. J. Yacaman, B. I. Yakobson, J. M. Tour, *Nat. Commun.* **2014**, *5*, 5714; b) M. F. El-Kady, R. B. Kaner, *Nat. Commun.* **2013**, *4*, 1475.

[19] G. Ye, Y. Gong, K. Keyshar, E. A. M. Husain, G. Brunetto, S. Yang, R. Vajtai, P. M. Ajayan, *Part. Part. Syst. Charact.* **2015**, *32*, 817.

[20] M. F. El-Kady, V. Strong, S. Dubin, R. B. Kaner, *Science* **2012**, *335*, 1326.

[21] a) J. Palenzuela, A. Viñuales, I. Odriozola, G. Cabañero, H. J. Grande, V. Ruiz, *ACS Appl. Mater. Interfaces* **2014**, *6*, 14562; b) E. Hwang, S. Seo, S. Bak, H. Lee, M. Min, H. Lee, *Adv. Mater.* **2014**, *26*, 5129.

[22] R. J. Mortimer, D. R. Rosseinsky, P. M. S. Monk, *Electrochromic Materials and Devices*, John Wiley & Sons, Inc., **2015**.

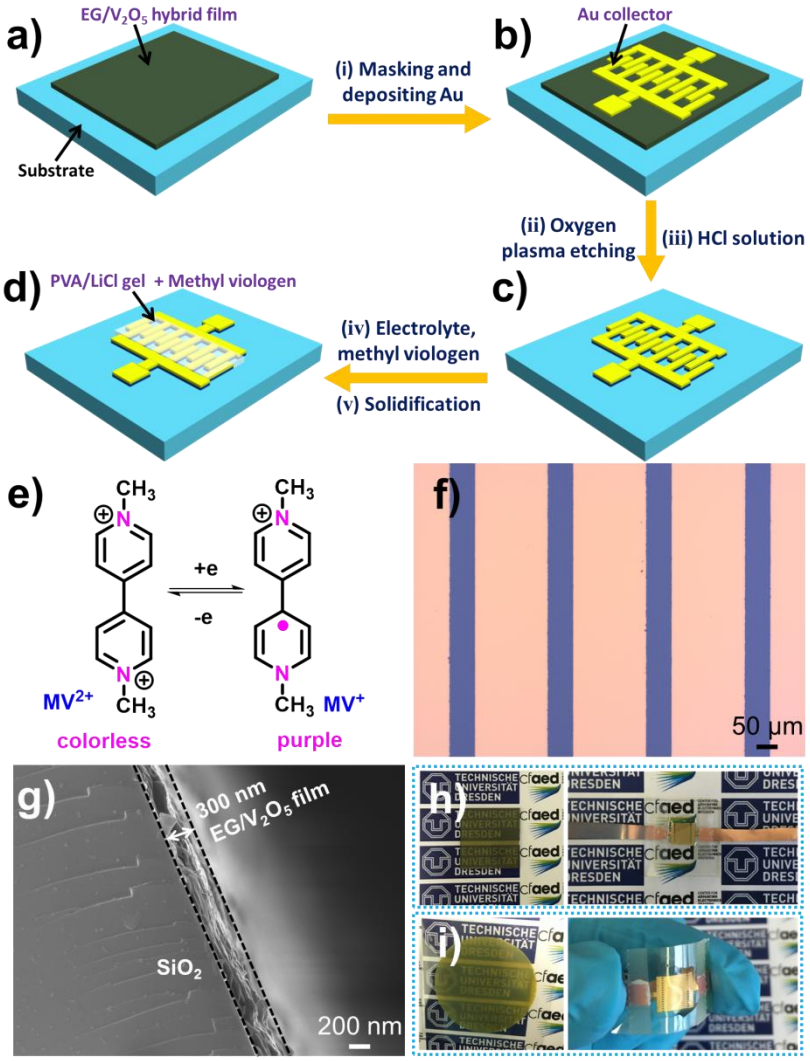

Figure 1. Schematic fabrication of SR-MSCs: (a) transferring EG/V_2O_5 nanopaper onto substrate; (b) masking and depositing gold current collector; (c) etching by O_2 plasma and HCl solution; (d) drop-casting and solidification of the viologen dissolved PVA/LiCl gel electrolyte. (e) The electrochromic mechanism of viologen (complex ions were not shown for clarity). (f) Optical image of the microelectrode pattern. (g) SEM image of glass-supported EG/V_2O_5 nanopaper profile. Digital photos of EG/V_2O_5 nanopaper and corresponding MSC devices (size: 1.5 cm × 1 cm) on glass (h) and PET (i) substrates.

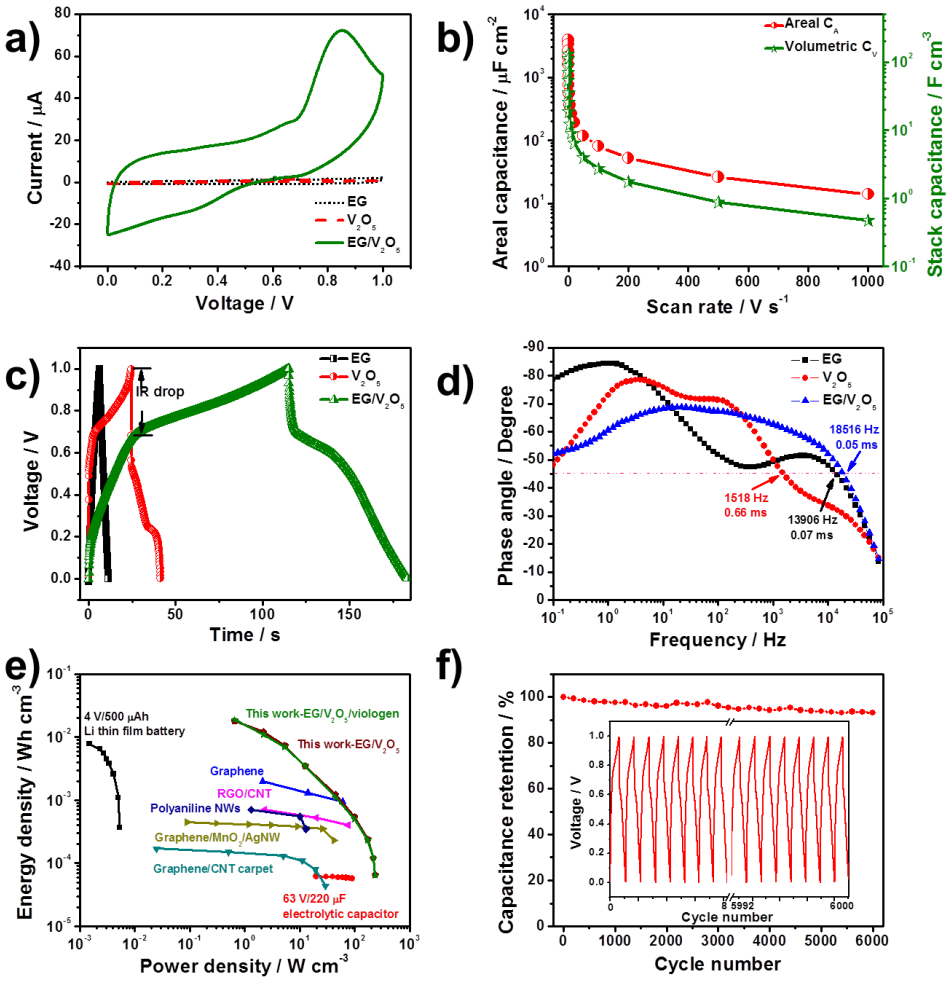

Figure 2. Electrochemical characterization of EG/V_2O_5-MSC. (a) CV curves of fabricated MSCs (EG film, V_2O_5 film, and EG/V_2O_5 hybrid film) at 10 mV s^{-1}. (b) Specific capacitances calculated from CV curves as function of scan rates. (c) GCD curves of MSCs at a current density of 0.02 mA cm^{-2}. (d) Impedance phase angle as function of the frequency for as-prepared MSCs. (e) Ragone plots for EG/V_2O_5-MSC (and EG/V_2O_5/viologen-MSC), reported Li thin film battery, activated carbon based electrolytic capacitor and graphene-based MSCs. (f) Cycling stability of EG/V_2O_5-MSC at the current density of 0.04 mA cm^{-2}. Inset shows the first eight and the last eight GCD curves of EG/V_2O_5-MSC.

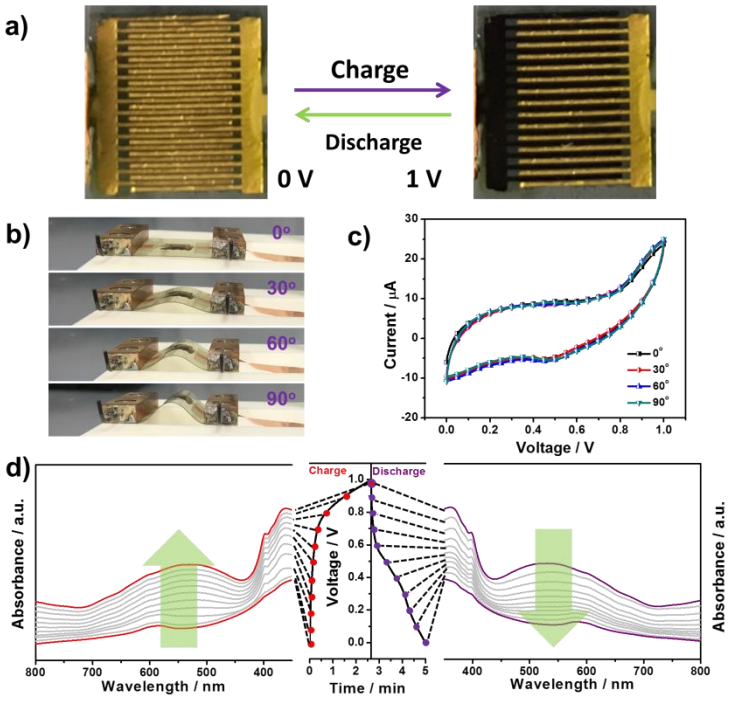

Figure 3. Stimulus-responsive performance of as-prepared flexible EG/V_2O_5-MSC (denoted as EG/V_2O_5-fMSC). (a) Photographs of the reversible electrochromic effect of EG/V_2O_5-fMSC during charge-discharge cycles (scale bar: 2000 μm). (b) Optical photos of the EG/V_2O_5-fMSC under different bending angles. (c) CV curves of the EG/V_2O_5-fMSC under different bending angles at a scan rate of 10 mV s^{-1}. (d) The UV-vis spectra of EG/V_2O_5-fMSC at different voltages at a current density of 0.01 mA cm^{-2} between 0 - 1.0 V during one charge-discharge cycle.

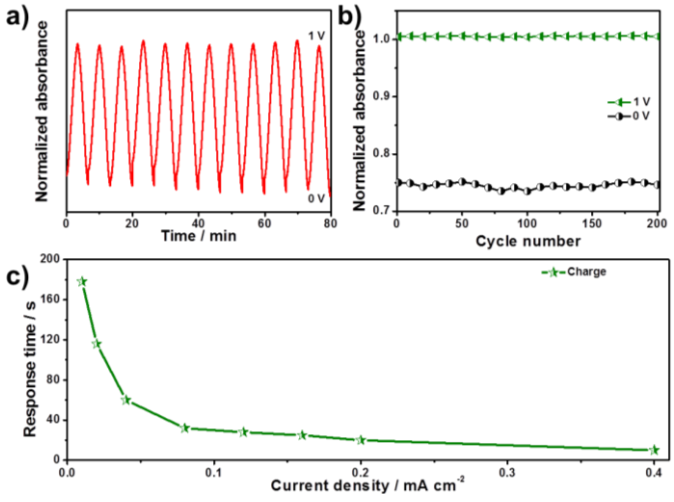

Figure 4. Stimulus-responsive performance of EG/V_2O_5-fMSC. (a) Voltage-controlled absorbance changes at 550 nm between 0 and 1.0 V for electrochromic EG/V_2O_5-fMSC. (b) Cycle stability of the electrochromic effect for EG/V_2O_5-fMSC. Inset is the voltage-controlled absorbance changes at 550 nm between 0 and 1.0 V for EG/V_2O_5-fMSC. (c) Response time for electrochromic effect as function of various current densities.